Journal of Power Sources 196 (2011) 4181–4186

Contents lists available at ScienceDirect

Journal of Power Sources

journal homepage: www.elsevier.com/locate/jpowsour

Evaluation of the R_2RuMnO_7 pyrochlores as cathodes in solid-oxide fuel cells

R. Martínez-Coronado[a], A. Aguadero[a,*], C. de la Calle[a], M.T. Fernández[b], J.A. Alonso[a]

[a] Instituto de Ciencia de Materiales de Madrid, C.S.I.C., Cantoblanco, E-28049 Madrid, France
[b] Institut Laue Langevin, BP 156X, Grenoble F-38042, France

ARTICLE INFO

Article history:
Received 28 July 2010
Received in revised form 27 August 2010
Accepted 27 August 2010

Keywords:
IT-SOFC
Cathode
Pyrochlore
R_2RuMnO_7

ABSTRACT

The use of pyrochlore oxides as solid-oxide fuel cells (SOFC) cathodes is a promising and rather unexplored alternative. The presence of some cationic disorder in pyrochlores promotes the Frenkel-defect formation responsible of a high-ionic conductivity in these compounds. Moreover, the use of the suitable transition metals at the B position gives rise to an adequate electronic conductivity constituting disordered pyrochlores as mixed, ionic–electronic conductors. In this work, we have synthesized and characterized a new family of pyrochlore oxides with the formula R_2MnRuO_7 (R = Tb, Dy, Ho, Er, Tm, Yb, Lu and Y) using the smallest rare-earth cations in order to promote disorder in the crystal lattice. Polycrystalline samples were prepared by a soft chemistry procedure involving citrates of the different metal ions, followed by thermal treatments in air or O_2 pressure. They are all cubic, space group $Fd\bar{3}m$. The Rietveld-refinement from neutron powder diffraction data at room-temperature evidences that the cation disorder (distribution of Mn between A and B positions) increases when the size of R decreases. This disorder is accompanied by an increment of the oxygen-vacancy concentration due to the reduction of Mn^{4+} at the B position to Mn^{2+} at the A position. The obtained compounds display a semiconductor-like behavior with a maximum conductivity of 8.9 S cm^{-1} for Er_2MnRuO_7 at 900 °C. Moreover, the measured thermal expansion coefficients are in the range of 9.8–10.7 × 10^{-6} K^{-1} between 100 and 900 °C that perfectly match those of the usual electrolytes, YSZ, LSGM or CGO. The obtained results present the R_2MnRuO_7 pyrochlores as alternative cathodes for IT-SOFCs.

1. Introduction

One of the biggest challenges to accomplish the development of solid-oxide fuel cells (SOFC) as economically viable energy-conversion devices is the decrease in the operating temperature (550–850 °C) without incurring in the deterioration of the effectiveness of the cell. The cathode is responsible for a significant drop in the cell potential at intermediate temperatures (550–850 °C), so the development of a mixed ionic–electronic conductor (MIEC) oxide to be used as a cathode with an appropriate conductivity is an important issue in solid state chemistry.

Co-based perovskites have been widely used as MIEC cathodes in intermediate temperature solid oxide fuel cells (IT-SOFC) [1–3]. $Ba_{0.5}Sr_{0.5}Co_{0.8}Fe_{0.2}O_{3-\delta}$ (BSCF) [4] and $SrCo_{0.8}Fe_{0.2}O_{3-\delta}$ (SCF) have been extensively studied due to their high oxygen fluxes and favourable oxygen-reduction performance at temperatures ≥600 °C [5,6]. However, these materials show moderate chemical stability, that could limit their performance at temperatures below 600 °C [7,8]. The $SrCo_{0.95}Sb_{0.05}O_{3-\delta}$ perovskite has been shown to be an excellent cathode with high electronic conductivity (500 S cm^{-1} at 400 °C) and very low polarization resistances [9,10]. However, Co-based perovskites are usually associated with a too high thermal expansion related to the other cell components.

Pyrochlore oxides with the composition $A_2B_2O_7$ are an extremely interesting alternative due to their high chemical and structural flexibility that allow tuning the adequate properties for specific applications. In general, pyrochlore oxides crystallize in the cubic, face-centered space group $Fd\bar{3}m$ [11], where the A cations are eightfold coordinated within scalenohedra (distorted cubes) that contains six equally spaced oxygen anions (O1) and two additional oxygen anions (O2) at a slightly shorter distance from the central cations. The smaller B cations are sixfold coordinated in trigonal antiprims (distorted octahedra) with all the six oxygen anions (O1) at equal distances of the central cation. The crystal structure of these oxides consists of a network of BO_6 octahedra that share vertices with angles B–O1–B near 130°, forming a system of interconnected tunnels. The pyrochlore structure can be considered as a superstructure of fluorite $(A,B)O_2$ where the ions A and B are long-distance ordered when their ionic radii are sufficiently different, at least for radius ratio $r_A/r_B > 1.46$. Pyrochlore oxides where A and B cations are fully ordered often have a poor conductivity of oxide anions. However, the presence of a cationic disorder favours the formation of Frenkel defects responsible of the oxide-ion diffusion

* Corresponding author. Tel.: +34 91 334 9000; fax: +34 91 372 0623.
E-mail addresses: ainara.aguadero@icmm.csic.es, ainara.aguadero@gmail.com (A. Aguadero).

0378-7753/$ – see front matter © 2010 Elsevier B.V. All rights reserved.
doi:10.1016/j.jpowsour.2010.08.091

in these materials [12,13]. In the $A_2B_2O_7$ pyrochlore structure, the A and B cations can undergo some antisite disordering in partially disordered structures. Regarding the nature of the cations at the B sites, Ru is an interesting element promoting good electrical and catalytic properties. A very good electrochemical behavior of Ru-based pyrochlores has been observed at temperatures as low as 350 °C, which has motivated its study as IT-SOFC cathodes [14,15]. However, Ru-based compounds as $A_2Ru_2O_7$ (A = Bi, Pb) have a high chemical instability with CGO or YSZ electrolytes [16,17]. On the other hand, Mn-based pyrochlores exhibit very interesting magnetic and electrical properties [18–20], Mn being, by far, less expensive than Ru. In this work we have prepared a new family of pyrochlores of stoichiometry R_2MnRuO_7 (R = Tb, Dy, Ho, Er, Tm, Yb, Lu and Y) in order to evaluate their potential use as IT-SOFC cathodes. We describe a comprehensive study of the crystal structure, thermal expansion and electrical conductivity of these materials.

2. Experimental

2.1. Sample preparation

R_2MnRuO_7 (R = Tb, Dy, Ho, Er, Tm, Yb, Lu and Y) was prepared by a wet chemistry procedure involving metal citrates. This method requires the formation of very reactive precursors starting from an aqueous solution of the metal ions in citric acid. Stoichiometric amounts of R_2O_3, $MnCO_3$ and RuO_2 were solved in citric acid and some drops of nitric acid. The solution was then slowly evaporated, leading to organic resins that contain a homogeneous distribution of the involved cations. The formed resins were dried at 120 °C and decomposed at 600 °C for 12 h and 800 °C for 2 h in order to eliminate the organic materials and the nitrates. This treatment gave rise to finely divided and homogeneous precursor materials that finally were heated in air at 900 °C for 12 h to obtain the pure pyrochlore oxide phase. For some rare-earth cations with small ionic radii a second treatment at 900 °C under 200 bar of oxygen pressure was needed to obtain the pure pyrochlore phase without the competitive $RMnO_3$ perovskite oxide (containing Mn^{3+}). Subsequent treatments at the same temperature for 12 h in air demonstrate that the obtained pyrochlores are stable in the usual working conditions of a SOFC cathode once formed. Further heat treatments at higher temperatures led to the formation of the mentioned perovskite oxides as secondary phases.

2.2. X-ray diffraction (XRD) and neutron diffraction data (NPD)

The initial characterization of the product was carried out by XRD with a Bruker-axs D8 Advanced diffractometer (40 kV, 30 mA), controlled by a DIFFRACT^{PLUS} software, in Bragg-Brentano reflection geometry with Cu Kα radiation (λ = 1.5418 Å) and a PSD (Position Sensitive Detector). A filter of nickel allows the complete removal of Cu Kβ radiation. The slit system was selected to ensure that the X-ray beam was completely within the sample for all 2θ angles. For the structural refinement NPD experiments were carried out in the high-resolution powder diffractometer D1A (λ = 1.91 Å) at the ILL in Grenoble. The patterns were collected in a displex unit at room-temperature (RT). About 2 g of sample were contained in a vanadium can; a time of 3 h was required to collect a full diffraction pattern. For the absorbing Dy compound a double-walled vanadium sample holder was utilized. The NPD data were analyzed by the Rietveld method [21] with the FULLPROF program [22]. A pseudo-Voigt function was chosen to generate the line shape of the diffraction peaks. The following parameters were refined in the final run: scale factor, background coefficients, zero-point error, pseudo-Voigt corrected for asymmetry parameters, positional coordinates and isotropic thermal factors for all the atoms.

2.3. Thermal expansion coefficient and electrical conductivity

Measurements of the thermal expansion coefficient and electrical conductivity required the use of sintered samples. Densification was performed by uniaxial pressing of pellets that were subsequently calcined at temperatures not higher than 900 °C for 12 h, in order to prevent the formation of secondary phases. The obtained density is around 70%. Thermal expansion of the sintered samples was performed in a dilatometer Linseis L75HX1000, between 100 and 900 °C in air. The conductivity was measured between 25 and 900 °C in air, by the four-point method in bar-shaped pellets under DC currents between 0.1 and 1 A. The currents were applied and collected with a Potentiostat–Galvanostat AUTOLAB PGSTAT 302 from ECO CHEMIE.

3. Results and discussion

3.1. Crystallographic characterization

The R_2MnRuO_7 oxides (R = Tb, Dy, Ho, Er, Tm, Yb, Lu and Y) were obtained as well-crystallized polycrystalline powders. The XDR diagrams shown in Fig. 1 are characteristic of a pyrochlore-type structure of formula $A_2B_2O_7$. They can be indexed in a cubic, face-centered unit-cell, as illustrated in Fig. 2 for Er_2RuMnO_7. No impurity phases were detected. To carry out a more accurate structural study of the R_2MnRuO_7 family, we performed a NPD investigation at RT for all the members of the series. The crystal structure of R_2MnRuO_7 is defined in the cubic $Fd\bar{3}m$ space group, with origin at (1/8, 1/8, 1/8). In this setting, the R cations are placed at 16*c* (1/2, 1/2, 1/2) sites, the Mn and Ru cations are distributed at random at 16*c* (0, 0, 0) position and the two kinds of nonequivalent oxygen atoms (O1 and O2) at 48*f* (*x*, 1/8, 1/8) and 8*b* (3/8, 3/8, 3/8) sites, respectively. In a second run some Mn atoms were allowed to be placed at the 16*c* positions together with R atoms (with the (R,Mn) occupancy constrained to unity), leading to a substantial improvement of the fit. The refinement of the mixed occupancy factors of the cations at A and B sublattices shows that there is a distribution of Mn between both positions which promote a degree of cationic disorder on the lattice. The occupancy of the O1 and O2 oxygen atoms was also refined, observing a significant deviation from the full stoichiometry in both positions which implies the presence of disordered oxygen vacancies into the lattice. Fig. 3 illus-

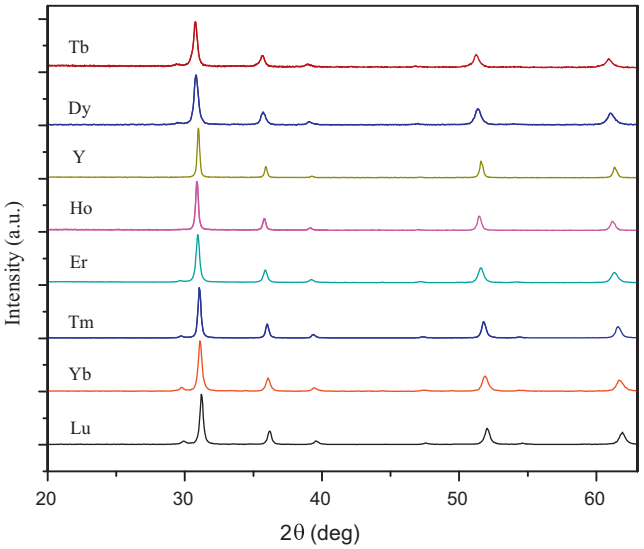

Fig. 1. XRD patterns for R_2RuMnO_7.

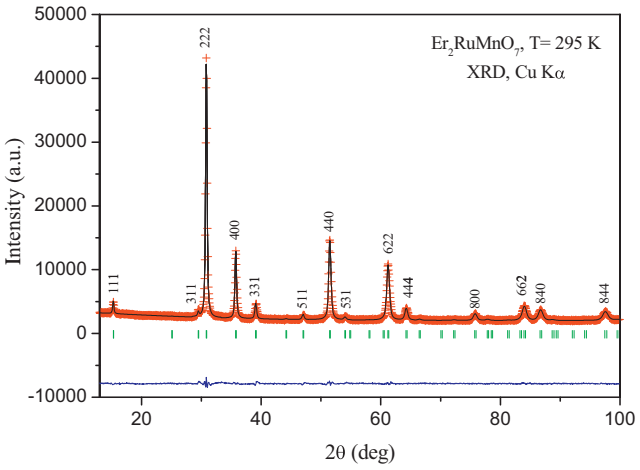

Fig. 2. XRD pattern of Er_2MnRuO_7, indexed in a cubic unit-cell.

trates the good agreement between the observed and calculated NPD patterns at RT for Y_2RuMnO_7, Er_2RuMnO_7, Tm_2RuMnO_7 and Lu_2RuMnO_7 and Table 1 summarizes the unit-cell, atomic, thermal parameters and discrepancy factors after the Rietveld-refinements of the different compounds. Table 2 contains the main interatomic distances and angles.

Fig. 4 illustrates the pyrochlore structure for R_2RuMnO_7 that can be described as two interpenetrating networks: the smaller (Ru,Mn) cations are octahedrally coordinated to O1-type oxygens, the $(Ru,Mn)O1_6$ octahedra sharing corners to give a $(Ru,Mn)_2O_{16}$ sublattice, which can be considered as the back-bone of the structure. The cage-like holes of this network contain a second sublattice $(R,Mn)_2O2$. It is worth noting that this network is not essential for the stability of the structure: both (R,Mn) and O2 atoms may be partially or totally absent, as it happens in certain families of defect pyrochlores AB_2O_6.

The lattice parameters of pyrochlore series R_2MnRuO_7 decrease as the ionic radius of rare-earth cation diminishes, as shown in Fig. 5a. This tendency is also observed for the $(R,Mn)_{16d}$–O interatomic distances and $(Ru,Mn)_{16c}$–O–$(Ru,Mn)_{16c}$ angles, which decrease along the series as shown in Fig. 5b. The obtained values for the $(Ru,Mn)_{16c}$–O interatomic distances are close to that expected from the ionic radii of Mn^{4+} (0.53 Å), Ru^{4+} (0.62 Å) and O^{-2} (1.40 Å) in a octahedral position [23] and are in perfect accordance with the expected interatomic distances extracted from the values presented by other authors for $R_2Mn_2O_7$ and $R_2Ru_2O_7$ oxides [24,25]. Very interestingly, Fig. 6 shows that the obtained degree of disorder (Mn at R positions) increases with decreasing the size of the involved rare-earth, which is in accordance with the tendency previously reported by García Casado et al. [26]. Moreover, the antisite disordering of Mn promotes the reduction of Mn^{4+} at the B position to Mn^{2+} at the A position, since the larger ionic-size

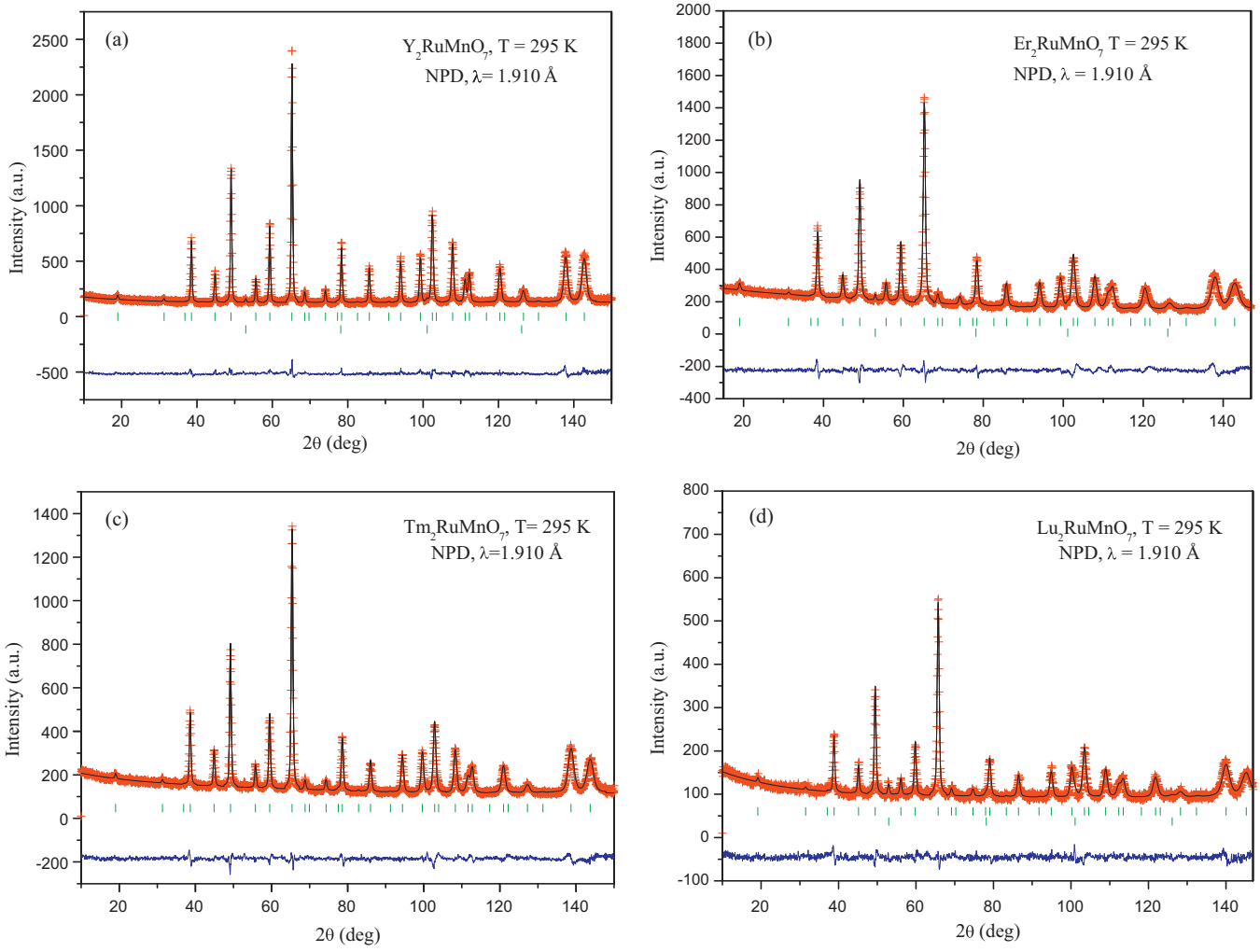

Fig. 3. Comparison of the observed (crosses), calculated (solid line), and difference (at the bottom) NPD patterns for, (a) Y_2RuMnO_7, (b) Er_2RuMnO_7, (c) Tm_2RuMnO_7 and (d) Lu_2RuMnO_7 at RT. The two series of tick marks correspond to the positions of the allowed Bragg reflections for the main phase and vanadium.

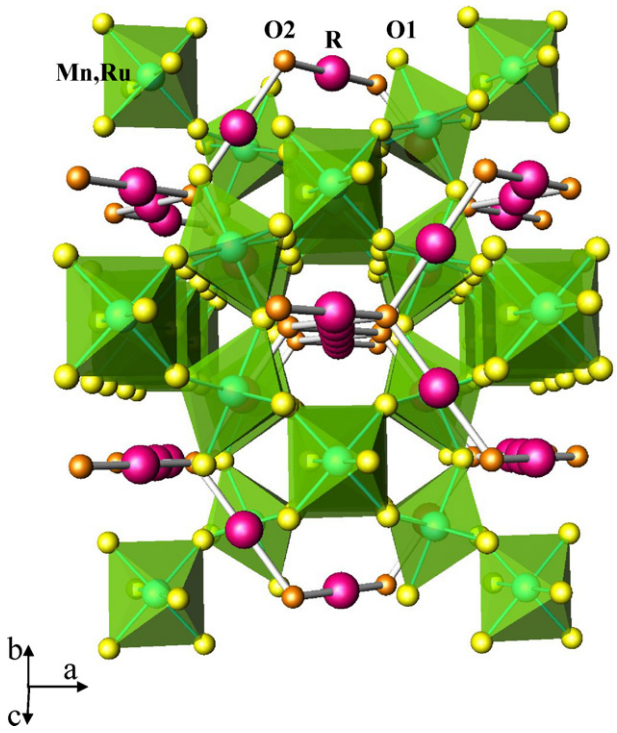

Fig. 4. Pyrochlore structure for R_2RuMnO_7.

of this Mn^{2+} ion (0.96 Å) is more adequate to occupy an eightfold oxygen-coordinated position. This implies, additionally, a hole-doping effect that involves the creation of oxygen vacancies (Fig. 7) that are expected to support the ionic conductivity, as usually observed in oxygen-defective perovskites. In fact, Fig. 7 shows an increment of the oxygen vacancies as the amount of Mn^{2+} at the 16*d* sublattice increases, excepting for Y that seems to be out of this trend.

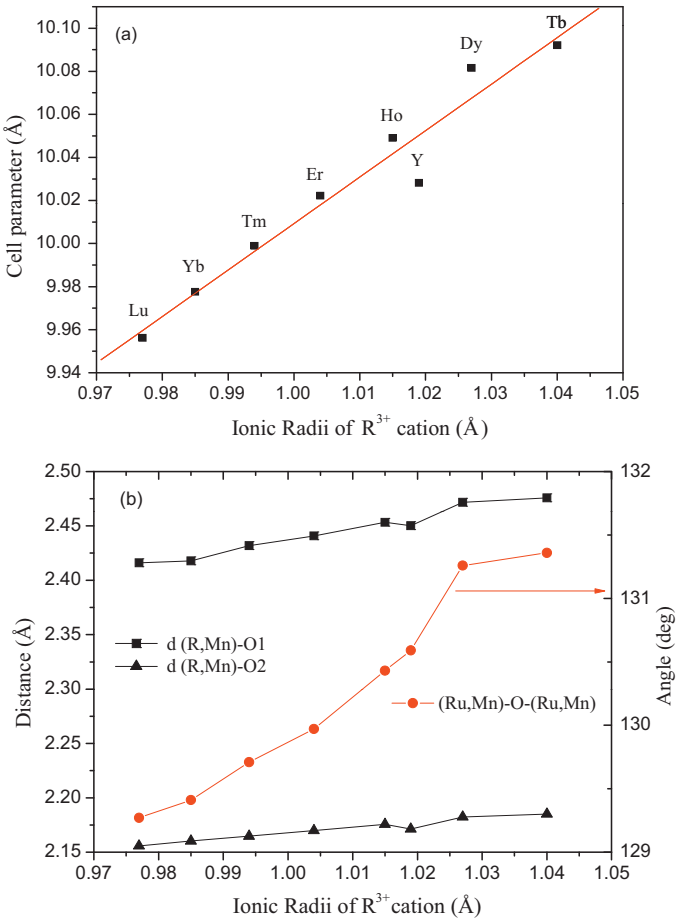

Fig. 5. (a) Variation of the unit-cell parameter and (b) of the $(R,Mn)_{16d}$–O interatomic distances and $(Ru,Mn)_{16c}$–O–$(Ru,Mn)_{16c}$ angles of R_2RuMnO_7 as a function of R^{3+} ionic radius.

Table 1
Unit-cell and thermal parameters for R_2RuMnO_7 in cubic $Fd\bar{3}m$ (no. 227) space group, from NPD at 295 K. (R,Mn) are placed at 16*d* (1/2, 1/2, 1/2), (Mn,Ru) at 16*c* (0, 0, 0), O1 at 48*f* (*x*, 1/8, 1/8) and O2 at 8*b* (3/8, 3/8, 3/8) positions.

R	Tb	Dy	Ho[a]	Y	Er	Tm	Yb	Lu
a (Å)	10.0921(7)	10.0816(6)	10.0491 (2)	10.0282(2)	10.0224(4)	9.9989(3)	9.9776(4)	9.9562(6)
V (Å^3)	1027.89(3)	1024.72(5)	1014.79 (3)	1008.16(3)	1006.68(4)	999.66(5)	993.29(3)	986.91(5)
(R,Mn) 16*d* (1/2, 1/2, 1/2)								
B_{iso} (Å^2)	0.751(1)	0.731(3)	0.381(2)	0.199(5)	0.359(8)	0.481(9)	1.035(7)	0.139(1)
f_{occ} (R)	0.97(2)	0.95(2)	0.94(4)	0.94(1)	0.93(0)	0.93(1)	0.92(0)	0.91(2)
f_{occ} (Mn)	0.03(2)	0.05(2)	0.06(2)	0.06(1)	0.07(0)	0.07(1)	0.08(0)	0.09(2)
(Ru,Mn) 16*c* (0, 0, 0)								
B_{iso} (Å^2)	0.531(3)	0.324(4)	0.524(6)	0.407(2)	0.572(3)	0.246(2)	0.253(3)	0.560(4)
f_{occ} (Ru)	0.50	0.50	0.50	0.50	0.50	0.50	0.50	0.50
f_{occ} (Mn)	0.47(2)	0.45(2)	0.44(1)	0.44(1)	0.43(2)	0.43(1)	0.42(0)	0.41(2)
O1 48*f* (*x*, 1/8, 1/8)								
x	0.32990(3)	0.33008(3)	0.33160(1)	0.33140(11)	0.33248(2)	0.33298(2)	0.33424(2)	0.33372(3)
B_{iso} (Å^2)	0.937(9)	0.480(1)	0.687(4)	0.172(4)	0.722(7)	0.770(6)	1.428(2)	0.555(2)
f_{occ}	0.98(8)	0.95(2)	0.94(3)	0.99(4)	0.93(6)	0.93(6)	0.93(2)	0.92(9)
O2 8*b* (3/8, 3/8, 3/8)								
B_{iso} (Å^2)	1.084(3)	0.218(3)	0.304(8)	0.210(9)	0.946(2)	0.596(2)	1.212(3)	0.268(3)
f_{occ}	0.99(2)	0.93(0)	0.93(1)	0.95(0)	0.94(1)	0.94(1)	0.93(0)	0.94(2)
Reliability factors								
χ^2	1.77	1.17	1.66	1.34	2.16	1.59	5.61	1.08
R_p (%)	3.81	2.99	3.07	3.87	3.67	3.78	6.60	3.79
R_{wp} (%)	5.05	3.85	4.22	4.95	4.84	4.90	8.46	4.90
R_{exp} (%)	3.80	3.56	3.08	4.27	3.30	3.89	3.57	4.70
R_{Bragg} (%)	6.13	9.44	2.71	2.67	5.61	5.96	6.03	7.66

[a] Taken from Ref. [20].

Table 2
Selected atomic distances (Å) and angles (°) for R_2RuMnO_7 at 295 K.

Distances/R	Tb	Dy	Ho[a]	Y	Er	Tm	Yb	Lu
(R,Mn)–O1 (*x*6)	2.4758(10)	2.4720(2)	2.4533(7)	2.4502(6)	2.4408(10)	2.4317(9)	2.4179(2)	2.416(2)
(R,Mn)–O2 (*x*2)	2.18500(9)	2.18273(8)	2.17569(2)	2.17117(2)	2.16987(5)	2.16483(4)	2.16021(5)	2.15558(8)
(Ru,Mn)–O1 (*x*6)	1.9578(8)	1.9565(2)	1.9566(7)	1.9514(5)	1.9550(8)	1.9526(7)	1.9538(2)	1.947(2)
Angles								
(Ru,Mn)–O1–(Ru,Mn)	131.36(4)	131.259(10)	130.43(2)	130.59(2)	129.97(3)	129.71(3)	129.41(8)	129.27(5)
O1–(Ru,Mn)–O1	83.36(5)	83.299(10)	82.65(3)	82.86(3)	82.46(5)	82.28(4)	81.852(8)	82.04(7)

[a] Taken from Ref. [20].

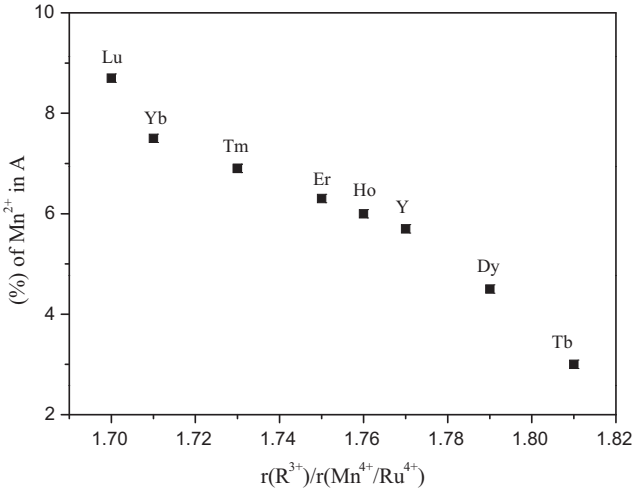

Fig. 6. Percentage of the Mn^{2+} in the A position of R_2RuMnO_7 as a function of the ionic radii of R.

3.2. Thermal expansion measurements

The thermal expansion of each pyrochlore phase was measured in pellets sintered at 900 °C. Fig. 8 shows a linear thermal expansion for all the R_2RuMnO_7 pyrochlore oxides with the absence of abrupt transitions in the entire temperature range measured. Table 3 contains the thermal expansion coefficient (TEC) values for the studied R_2RuMnO_7 oxides. The TECs of the sintered samples exhibit values that range from 9.8 to $10.7 \times 10^{-6}\,K^{-1}$ between 100 and 900 °C, which perfectly match the thermal expansions of the other components of a SOFC and are in accordance with the values previously reported for Ru-based pyrochlores [27].

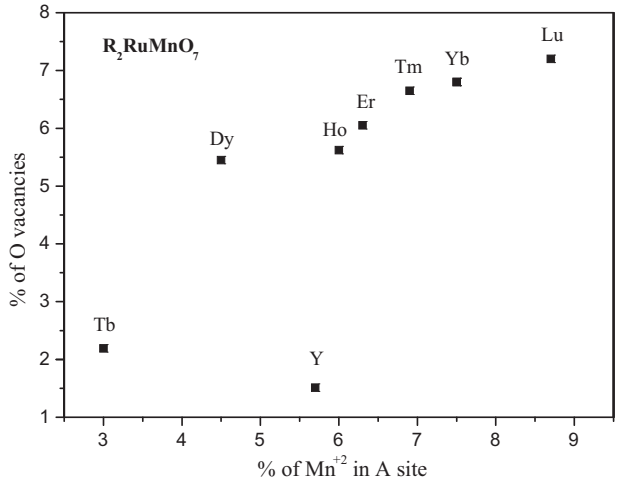

Fig. 7. Total vacancies of oxygen as a function of the percentage of Mn^{2+} in the A position.

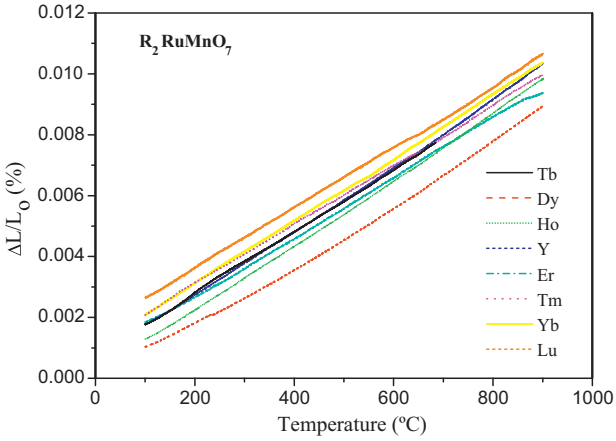

Fig. 8. Thermal expansion of R_2RuMnO_7.

3.3. Electrical conductivity measurements

Fig. 9 shows the thermal variation of the conductivity of all the pyrochlore oxides under study. The variation of the conductivity with temperature was analyzed after the Arrhenius law, according to the expression:

$$\sigma_{dc}T = (\sigma_o)\exp\left(\frac{-E_{dc}}{k_bT}\right)$$

where σ_o and E_{dc} are respectively the pre-exponential factor (related with the effective number of mobile transport charge) and the activation energy for the conductivity process. All the prepared materials display a semiconducting behavior in the whole range of measured temperatures. Fig. 9 evidences a change of the slope for all the compositions under study and therefore, two fits were per-

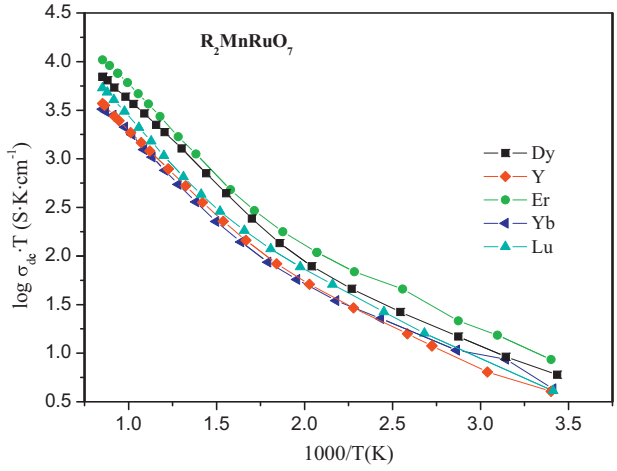

Fig. 9. Thermal evolution of the electrical conductivity for the R_2RuMnO_7 series.

Table 3
Thermal expansion coefficients for R_2RuMnO_7 between 100 and 900 °C.

R	Tb	Dy	Y	Ho	Er	Tm	Yb	Lu
$TEC_{100-900}$ ($\times 10^{-6}$ K^{-1})	10.13	10.02	10.69	10.76	9.82	9.74	10.31	9.88

formed for the 25–300 °C and 300–900 °C temperature ranges. The electrical conductivity shows a similar trend in all the composition under measurements. The maximum values obtained vary from 8.9 for Er_2MnRuO_7 to 3.2 S cm^{-1} for Yb_2 $MnRuO_7$ at 900 °C showing little correlation with the rare-earth ionic radius, although there is a trend to increase for the intermediate ionic-size lanthanide ions (Er, Dy). However, it cannot be excluded that the observed differences are related to the compactness or sintering level of the different compounds. At 750 °C, the conductivity spans from 2.1 to 6.6 S cm^{-1}. It is important to note that the conductivity values are probably underestimated due to the difficulty in the densification of the samples. The activation energies for the 25–300 °C and 300–900 °C temperature ranges exhibit values between 0.16–0.18 and 0.35–0.38 eV, respectively.

Ru-based pyrochlores with Bi or Pb in the A position have been observed to be metallic conductors with Pauli paramagnetism and low resistivity values (10^{-2} Ω cm) [16,25]. When Bi and/or Pb are substituted by a rare-earth (Pr–Lu and Y) a transition from metallic to semiconducting behavior accompanied by an increase of the resistivity is observed. This variation in the electrical behavior has been correlated to the structural features induced by the rare-earths in the A position. In particular, the electrical behavior of Ru-based pyrochlores have been correlated with geometrical considerations in such a way that metallic behaviors have been associated with (Ru)–O–(Ru) angles higher than 133° and Ru–O distances shorter than 2 Å [28–30]. The obtained R_2MnRuO_7 family of compounds displays highly distorted structures with (Ru,Mn)–O–(Ru,Mn) angles that varies from 131 to 129° that in accordance with the geometric considerations promotes a semiconducting-like behavior of the electrical conductivity. The introduction of Mn in the crystal lattice highly diminish the cost of these materials and promotes the creation of disordered oxygen vacancies due to the reduction of Mn^{4+} to Mn^{2+} that is introduced in the A position. These vacancies would provide to these materials with the adequate ionic conductivity to be used as MIEC. However, the presence of some amount of Ru in the crystal structure is important in order to increment the low electrical conductivity usually observed in R_2MnO_7 pyrochlores [24].

4. Conclusion

We have synthesized a new series of pyrochlore oxides of stoichiometry R_2MnRuO_7 (R = Tb, Dy, Ho, Er, Tm, Yb, Lu and Y), exhibiting a cubic $Fd\bar{3}m$ symmetry. The refinement of the occupancy factors of the cations shows a certain degree of disorder of Mn between A and B positions, which increases as the rare-earth radii diminishes. At A positions Mn exhibits a divalent oxidation state, whereas it is tetravalent at the B sites. The increment of the amount of Mn at A sites is concomitant with the increment of concentration of disordered oxygen vacancies in these oxides, which is expected to provide them with the required ionic mobility to be used as cathodes in SOFCs. The electrical characterization evidences a semiconducting behavior in these oxygen-defective pyrochlores. The highest conductivity is presented by Er_2MnRuO_7 reaching a value of 8.9 S cm^{-1} at 900 °C. The measured thermal-expansion coefficients display values of 9.8–10.7 $\times$ 10^{-6} K^{-1} between 100 and 900 °C that perfectly match with those of other SOFC components, making them a promising alternative as possible cathodes in solid-oxide fuel cells of intermediate temperature.

Acknowledgements

We thank the financial support of the Spanish Ministry of Science and Innovation (MICINN) to the projects Grant Nos. MAT2007-60536-06 and MAT2008517-01-C02 and we are grateful to the Institut Laue Langevin (ILL) in Grenoble for making all facilities available. A.A. also wants to thank MICINN for the contract "Juan de la Cierva".

References

[1] T. Nagai, W. Ito, T. Sakon, Solid State Ionics 177 (2007) 3433–3444.
[2] Z.Q. Deng, W. Liu, C.S. Chen, H. Lu, W.S. Yang, Solid State Ionics 170 (2004) 187–190.
[3] P. Zeng, R. Ran, Z. Chen, W. Zhou, H. Gu, Z. Shao, S. Liu, J. Alloys Compd. 455 (2008) 465–470.
[4] Z.P. Shao, S.M. Haile, Nature 431 (2004) 170–173.
[5] W. Zhou, R. Ran, Z. Shao, J. Power Sources 192 (2009) 231–246.
[6] J.J. Tunney, M.L. Post, X. Du, D. Yang, J. Electrochem. Soc. 149 (2002) 113–118.
[7] S. Svarcova, K. Wiik, J. Tolchard, H.J.M. Bouwmeester, T. Grande, Solid State Ionics 178 (2008) 1787–1791.
[8] E. Bucher, A. Egger, G.B. Caraman, W. Sitte, J. Electrochem. Soc. 155 (2008) B1218–B1224.
[9] A. Aguadero, D. Pérez-Coll, C. De la Calle, J.A. Alonso, M.J. Escudero, L. Daza, J. Power Sources 192 (2009) 132–137.
[10] A. Aguadero, J.A. Alonso, C. de la Calle, M.T. Fernández-Díaz, J.B. Goodenough, Chem. Mater. 22 (2010) 789–798.
[11] M.A. Subramanian, G. Aravamudan, G.V. Subba Rao, Prog. Solid State Chem. 15 (1983) 55.
[12] J.A. Díaz-Guillén, M.R. Díaz-Guillén, K.P. Padmasree, A.F. Fuentes, J. Santamaría, C. León, Solid State Ionics 179 (2008) 2160–2164.
[13] P.J. Wilde, C.R.A. Catlow, Solid State Ionics 112 (3–4) (1998) 173–183.
[14] J.B. Goodenough, R. Manoharan, P. Paranthaman, J. Am. Chem. Soc. 112 (1990) 2076–2082.
[15] H.S. Horowitz, J.M. Longo, H.H. Horowitz, J. Electrochem. Soc. 130 (9) (1983) 1851–1859.
[16] G. Ehora, S. Daviero-Minaud, M.C. Steil, L. Gengembre, M. Frère, S. Bellayer, O. Mentrè, Chem. Mater. 20 (24) (2008) 7425–7433.
[17] R. Doshi, V.L. Richards, J.D. Carter, X. Wang, M. Krumpelt, J. Electrochem. Soc. 146 (4) (1999) 1273–1278.
[18] Y. Shimakawa, Y. Kubo, T. Manako, Nature 379 (1996) 53–55.
[19] Y. Shimakawa, Y. Kubo, Mater. Sci. Eng. B 63 (1999) 44–48.
[20] M. Retuerto, M.J. Martínez-Lope, C. de la Calle, R. Martínez-Coronado, M. García-Hernández, M.T. Fernández, J.A. Alonso, J. Appl. Phys. 107 (9) (2010), 093919-093919-7.
[21] H.M. Rietveld, J. Appl. Crystallogr. 2 (1969) 65–71.
[22] J. Rodríguez-Carvajal, Physica B 192 (1993) 55–69.
[23] R.D. Shannon, Acta Crystallogr. A 32 (1976) 751–756.
[24] M.A. Subramanian, C.C. Torardi, D.C. Johnson, J. Pannetier, A.W. Sleight, J. Solid State Chem. 74 (1988) 24–30.
[25] T. Nobuyuki, M. Wakeshima, Y. Hinatsu, A. Tobo, K. Ohoyama, J. Solid State Chem. 176 (2003) 165–169.
[26] P. García Casado, J.A. Alonso, J.L. Martínez, M.T. Fernández, I. Rasines, Chem. Mater. 12 (5) (2000) 1217–1221.
[27] T. Takeda, R. Kanno, Y. Kawamoto, Y. Takeda, O. Yamamoto, J. Electrochem. Soc. 147 (5) (2000) 1730–1733.
[28] R. Kanno, Y. Takeda, T. Yamamoto, Y. Kawamoto, O. Yamammoto, J. Solid State Chem. 1025 (1993) 106–114.
[29] H. Kobayashi, R. Kanno, Y. Kawamoto, T. Kamiyama, A.W. Sleight, J. Solid State Chem. 114 (1995) 15–23.
[30] T. Yamamoto, R. Kanno, Y. Takeda, O. Yamamoto, Y. Kawamoto, M. Takano, J. Solid State Chem. 109 (1994) 372–383.